

Sensing Security Oriented OFDM-ISAC Against Multi-Intercept Threats

Lingyun Xu, *Graduate Student Member IEEE*, Bowen Wang, *Graduate Student Member IEEE*,
Huiyong Li and Ziyang Cheng, *Senior Member IEEE*

Abstract—In recent years, security has emerged as a critical aspect of integrated sensing and communication (ISAC) systems. While significant research has focused on secure communications, particularly in ensuring physical layer security, the issue of sensing security has received comparatively less attention. This paper addresses the sensing security problem in ISAC, particularly under the threat of multi-intercept adversaries. We consider a realistic scenario in which the sensing target is an advanced electronic reconnaissance aircraft capable of employing multiple signal interception techniques, such as power detection (PD) and cyclostationary analysis (CA). To evaluate sensing security under such sophisticated threats, we analyze two critical features of the transmitted signal: (i) power distribution and (ii) cyclic spectrum. Further, we introduce a novel ergodic cyclic spectrum metric which leverages the intrinsic mathematical structure of cyclostationary signals to more comprehensively characterize their behavior. Building on this analysis, we formulate a new ISAC design problem that explicitly considers sensing security, and we develop a low-complexity, efficient optimization approach to solve it. Simulation results demonstrate that the proposed metric is both effective and insightful, and that our ISAC design significantly enhances sensing security performance in the presence of multi-intercept threats.

Index Terms—Low probability of intercept, orthogonal frequency division multiplexing, multiple-input multiple-output, integrated sensing and communication, hybrid beamforming

I. INTRODUCTION

A. Context and Motivation

INTEGRATED sensing and communication (ISAC) systems support both communication and sensing functionalities within a unified framework by sharing signal processing modules, frequency bands, and hardware resources. This integration significantly improves spectrum efficiency and reduces hardware costs [1]–[3]. Thanks to these advantages, ISAC has attracted increasing attention as a key enabler for future 6G applications, including vehicle-to-everything, smart homes, and environmental monitoring [4]–[6].

Despite these advancements, security remains a critical and underexplored issue in ISAC systems, stemming from the inherent broadcast nature and spectrum-sharing mechanisms [7]. In particular, the dual objectives of communication and sensing introduce unique security challenges from two perspectives: secure communication and secure sensing.

L. Xu, H. Li and Z. Cheng are with the School of Information and Communication Engineering, University of Electronic Science and Technology of China, Chengdu 611731, China. (email: xusherly@std.uestc.edu.cn, hyl@uestc.edu.cn, zycheng@uestc.edu.cn).

B. Wang is with the King's Communications, Learning and Information Processing lab, King's College London, London, WC2R 2LS, UK. (email: bowen.wang@kcl.ac.uk)

In terms of secure communication within ISAC systems, where the objective is to prevent information leakage and ensure data confidentiality, extensive research efforts have been devoted, particularly in the domains of physical layer security [8]–[15]. These studies primarily focus on mitigating the risk of eavesdropping by unauthorized entities. To achieve this, various techniques have been proposed, including artificial noise injection [16]–[18], cooperative jamming [19]–[21], and constellation shaping [22]–[24], all aimed at degrading the reception quality at potential eavesdroppers while preserving reliable communication for legitimate users.

Sensing security refers to the ability of a system to conduct sensing operations without being easily detected, intercepted, or exploited by adversaries [25], [26]. When sensing security is taken into account in ISAC systems, conventional methods that prioritize sensing accuracy are no longer sufficient. Instead, low-probability-of-intercept (LPI) strategies [25], [27], [28] should be exploited to minimize the risk of signal interception while ensuring reliable sensing performance. A lack of LPI features in ISAC signals may allow electronic surveillance systems (ESMs) to detect and localize transmission over long distances, thereby compromising the stealth and integrity of the sensing task [25]–[28]. Compared to communication insecurity, which typically results in data leakage or service disruption, sensing insecurity can entail significantly more severe consequences, including the potential exposure of the ISAC platform's location, operational status, or strategic intent.

Although sensing security is critical for real-world ISAC applications, it has received disproportionately less attention compared to its communication counterpart and remains largely underexplored. Motivated by this critical gap, we conduct a comprehensive investigation into sensing security for ISAC, focusing on performance analysis under multi-intercept threats, and beamforming design strategies.

B. Related Work and Challenges

The design of LPI strategies for ISAC systems is closely related to the capabilities of electronic reconnaissance (ER) platforms. In general, ER systems can be categorized based on their interception mechanisms: (i) power detection (PD)-based ERs that monitor signal strength, and (ii) feature extraction-based ERs that exploit signal structures such as modulation, time-frequency signatures (TFS), or cyclostationary features.

1) *ISAC Against Power Detection-Based Interception*: PD-based ER systems detect transmissions by evaluating the received signal's power spectral density. To counter such

threats, power-constrained sensing has been proposed, aiming to minimize the radiated power of ISAC signals [29]–[32]. For instance, an optimal power allocation framework was proposed in [30], where the transmit power across multiple ISAC transmitters was minimized subject to constraints on target detection and communication throughput. Similarly, the authors in [31] designed a power allocation strategy for target time-delay estimation, minimizing radar power consumption while maintaining both estimation accuracy and communication quality-of-service (QoS). While reducing transmit power naturally lowers the probability of interception by ER with PD, it also inevitably compromises sensing performance.

2) ISAC Against Feature Extraction-Based Interception:

To defend against more advanced ER systems that employ cyclostationary or TFS to extract intrinsic features of the transmitted signals, even under low power conditions [33]–[35], feature-obfuscated sensing methods have been proposed. For example, to combat cyclostationary analysis (CA), authors in [36] proposed a reconfigurable intelligent surface (RIS)-aided waveform design, where the Cramér-Rao bound for extracting cyclic spectrum elements was minimized subject to radar detection and communication QoS constraints. Moreover, authors in [37] investigated the LPI design for multiple-input multiple-output (MIMO) ISAC systems combating an ER target and multiple jammers, where the transmit waveform and communication precoder were optimized by maximizing radar SINR while guaranteeing communication SINR and suppressing the cyclic frequency sidelobe level.

Despite several initial attempts toward enabling secure sensing in ISAC systems, multiple technical challenges remain unresolved:

- *Uncertainty in ER decision-making:* Most existing methods rely on fixed or known ER detection decision-making mechanisms, limiting their adaptability and robustness in adversarial or dynamically changing environments.
- *Multi-intercept threats:* Modern ER platforms may simultaneously employ multiple intercept strategies, such as PD and CA, necessitating more comprehensive and resilient ISAC design strategies.

These challenges underscore the necessity for a robust, system-level ISAC framework capable of defending against heterogeneous and evolving intercept threats—a gap this pioneering work aims to address.

C. Contributions

The main contributions of this work are summarized as follows.

- *Sensing Security Analysis and Insights:* An advanced ER aircraft employing multiple intercept processing methods, i.e., PD and CA, is considered. Under this practical interception setting, the sensing security problem is systematically investigated, where detailed analyses of the intercepted signals are conducted in terms of both received power and cyclic spectrum features. Through this comprehensive analysis, several critical insights are obtained regarding the sensing vulnerability of ISAC signals under multi-intercept threats. Furthermore, by exploring

the intrinsic mathematical properties of the ergodic cyclic spectrum matrix, a new design guideline is established to ensure the full emulation of cyclostationary behavior, thereby overcoming the limitations of conventional partial feature-based approaches.

- *Robust Security-Aware ISAC System.* Since the specific internal decision-making mechanisms by which the ER aircraft integrates information to determine interception is inaccessible, ISAC systems need to possess inherent robustness and security awareness. With the sensing security analysis at hand, the ISAC system should: 1) operate with reduced radiated power, thereby limiting its electromagnetic visibility; 2) enforce a cyclic spectrum that closely resembles background noise, thereby degrading the effectiveness of distinguishing signal features from noise. These capabilities enhance sensing security and robustness of ISAC systems under complex conditions, even when the decision-making mechanisms of the ER aircraft are unknown or potentially evolving.
- *Low-Complexity Design and Performance Evaluation.* Guided by our analysis and design insights, we formulate a practical beamforming design problem to enable secure sensing in ISAC systems. To tackle the high-dimensional non-convex design problem, we propose an effective algorithm to optimize the transmit beamformer and radar receive filter alternatively based on the alternating optimization method. Finally, we provide numerical simulations to assess the performance of the proposed design, validating the convergence of the proposed algorithm and the effectiveness in guaranteeing satisfactory communication and sensing performance. It also shows the superiority of the proposed LPI-aware secure OFDM-ISAC system over the conventional schemes in suppressing radiated power and generating noise-like cyclic spectra.

D. Organization and Notations

1) *Organization:* Section II introduces the system model. Section III presents the security sensing performance analysis. Section IV formulates the sensing security oriented OFDM-ISAC problem and Section V devises the LPI design against multi-intercept threats and proposes an effective algorithm. Section VI demonstrates the numerical simulations. Section VII concludes this work.

2) *Notations:* This paper uses a , \mathbf{a} and \mathbf{A} for scalars, vectors and matrices, respectively. $\mathbf{A}(i, j)$ denotes an element in the i -th row and the j -th column of \mathbf{A} . \mathbb{C}^n denotes an n dimensional complex-valued vector and $\mathbb{C}^{m \times n}$ denotes an m by n dimensional complex-valued space. $(\cdot)^T$ and $(\cdot)^H$ denote the transpose and conjugate transpose operators, respectively. $|\cdot|$ represents a determinant or absolute value determined by the context. $\|\cdot\|_F$ and $\text{Tr}(\cdot)$ denote the Frobenius norm and trace, respectively. $\mathbb{E}\{\cdot\}$ denotes expectation. $\Re\{\cdot\}$ denotes the real part of a complex-valued number. $\mathcal{CN}(0, \mathbf{R})$ denotes the complex Gaussian distribution with zero mean and covariance \mathbf{R} . $\text{Diag}(\cdot)$ denotes forming diagonal matrix from the input.

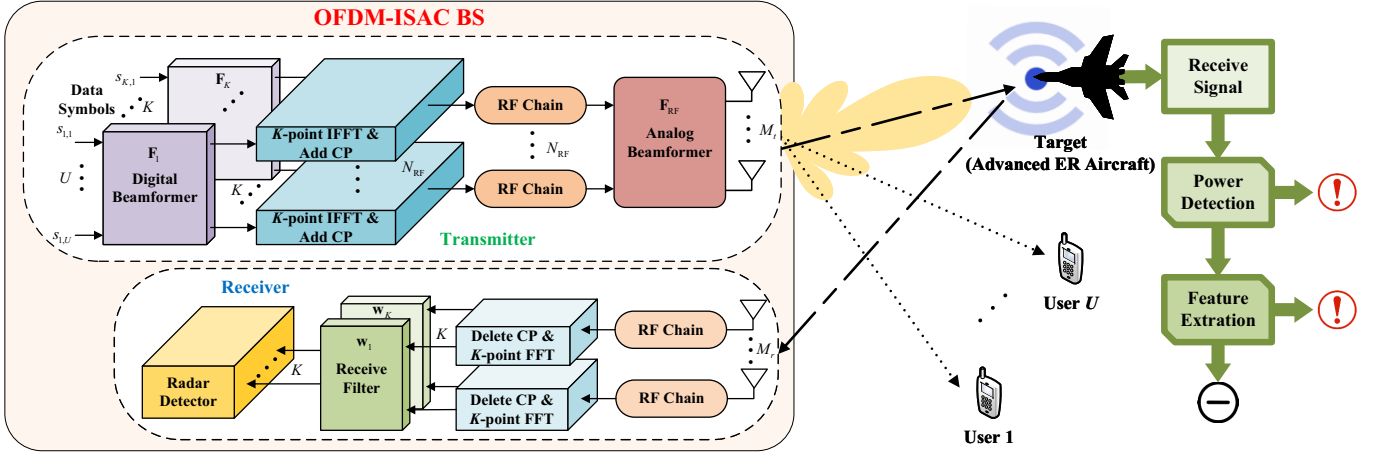


Fig. 1. An illustration of an OFDM-ISAC system with hybrid beamforming architecture at the transmitter in the presence of an advanced ER aircraft.

II. SYSTEM MODEL

As shown in Fig. 1, we consider an OFDM-ISAC base station (BS) with K subcarriers, which serves U single-antenna communication users while simultaneously probing a single-antenna target of interest. Specifically, the transmitter is equipped with M_r antennas and the colocated radar receiver is equipped with M_r receive antennas. They both adopt uniform linear arrays (ULAs), with the element spacing d .

A. Transmission Model

To cut down the tremendous power consumption and hardware overhead introduced by massive MIMO techniques, the transmitter adopts a hybrid beamforming architecture with N_{RF} RF chains [38], [39]. The transmit data symbol at the k -th subcarrier is denoted by $\mathbf{s}_k = [s_{k,1}, \dots, s_{k,U}]^T \in \mathbb{C}^U$, assuming $\mathbb{E}\{\mathbf{s}_k \mathbf{s}_k^H\} = \mathbf{I}_U$. The data symbol is firstly processed by the digital beamformer $\mathbf{F}_k = [\mathbf{f}_{k,1}, \dots, \mathbf{f}_{k,U}] \in \mathbb{C}^{N_{\text{RF}} \times U}$ in the frequency domain. Then, the signals are converted to the time domain by N_{RF} K -point inverse fast Fourier transforms (IFFTs) and added with the cyclic prefix (CP). After the up-conversion to the radio frequency (RF) domain by N_{RF} RF chains, the analog signals are processed by the analog beamformer $\mathbf{F}_{\text{RF}} \in \mathbb{C}^{M_t \times N_{\text{RF}}}$ implemented by phase shifters (PSs), i.e., $[\mathbf{F}_{\text{RF}}]_{i,j} = 1, \forall i, j$. Finally, the ISAC signals are emitted by M_t antennas. Therefore, the transmitted signal from the OFDM-ISAC BS at the time instant $t \in [0, \Delta t]$ is given by

$$\mathbf{x}(t) = \mathbf{F}_{\text{RF}} \sum_{k=1}^K \mathbf{F}_k \mathbf{s}_k e^{j2\pi f_k t}, \quad (1)$$

where $f_k = f_c + (k - K/2)\Delta f$ denotes the frequency at the k -th subcarrier, with the center frequency f_c , the subcarrier spacing $\Delta f = B/K = 1/\Delta t$, and the system bandwidth B .

B. Reception Model

1) *Communication Reception Model*: For the downlink communication, the received signal at the u -th user at the k -th subcarrier is given by

$$r_{k,u} = \mathbf{h}_{k,u}^H \mathbf{F}_{\text{RF}} \mathbf{f}_{k,u} \mathbf{s}_k + \sum_{i \neq u} \mathbf{h}_{k,u}^H \mathbf{F}_{\text{RF}} \mathbf{f}_{k,i} \mathbf{s}_k + n_{k,u}, \quad (2)$$

where $n_{k,u}$ denotes the complex additive white Gaussian noise (AWGN) with power spectral density σ_C^2 , $\mathbf{h}_{k,u} \in \mathbb{C}^{M_t}$ denotes the channel state information (CSI) vector from the transmitter to the u -th user at the k -th subcarrier [40]–[42].

2) *Radar Reception Model*: In this paper, the radar receiver co-located with the transmitter needs to collect the echo signals in order to detect the target of interest. Assume an advanced ER aircraft is located at the angle θ_E . The received signal is down-converted via M_t RF chains. After removing the CPs and transforming the time-domain signal into the frequency domain via M_r K -point fast Fourier transforms (FFTs), the signal is processed by the receive filter $\mathbf{w}_k \in \mathbb{C}^{M_r}$. The output signal is given by

$$\tilde{y}_{\text{R},k} = \mathbf{w}_k^H \varsigma_E \mathbf{A}(\theta_E, f_k) \mathbf{F}_{\text{RF}} \mathbf{F}_k \mathbf{s}_k + \mathbf{w}_k^H \mathbf{z}_{\text{R},k}, \quad (3)$$

where $\mathbf{z}_{\text{R},k} \sim \mathcal{CN}(0, \sigma_{\text{R}}^2 \mathbf{I}_{M_r})$ denotes the AWGN, ς_E denotes the complex amplitude of the ER aircraft, and $\mathbf{A}(\theta, f_k) = \mathbf{a}_r(\theta, f_k) \mathbf{a}_t^H(\theta, f_k)$, with the space-frequency transmit and receive steering vectors $\mathbf{a}_t(\theta, f) = \frac{1}{\sqrt{M_t}} [e^{j2\pi f \tau_1}, e^{j2\pi f \tau_2}, \dots, e^{j2\pi f \tau_{M_t}}]^T \in \mathbb{C}^{M_t}$ and $\mathbf{a}_r(\theta, f) = \frac{1}{\sqrt{M_r}} [e^{j2\pi f \tau_1}, e^{j2\pi f \tau_2}, \dots, e^{j2\pi f \tau_{M_r}}]^T \in \mathbb{C}^{M_r}$, respectively. $\tau_m = (m - 1)d \sin \theta / v$, and v is electromagnetic wave speed.

3) *ER Aircraft Reception Model*: Suppose there exists an advanced ER aircraft that employs the broad-beam and wide-band reception modes to passively receive the surrounding signals. The signal received by the advanced ER aircraft at the k -th subcarrier is given by

$$r_k = \alpha_k \mathbf{a}_t^H(\theta_E, f_k) \mathbf{F}_{\text{RF}} \mathbf{F}_k \mathbf{s}_k + n_{\text{E},k}, \quad (4)$$

where $n_{\text{E},k}$ denotes the AWGN with power spectral density σ_{E}^2 , α_k denotes the complex path loss coefficient.

III. SENSING SECURITY PERFORMANCE ANALYSIS

In this section, we focus on the analysis of sensing security performance. We first analyze the properties of intercepted signals and then exploit the properties to obtain a feasible LPI design guideline.

Before starting our analysis, it is essential to first clearly introduce the sensing security challenges in the presence of the advanced ER aircraft. As shown in Fig. 1, in this paper,

we assume that the advanced ER aircraft can scan and receive signals emitted from the OFDM-ISAC BS and then perform multiple intercept processing methods: 1) *PD*: By measuring whether the power of the received signal exceeds a preset threshold, the ER aircraft can determine the existence of radar signals [26]. 2) *CA*: By analyzing the cyclostationary of the received signals, the ER aircraft can distinguish the radar signals from the background noise [26]. Such a complex scenario significantly complicates the task of ensuring sensing security in ISAC systems, as the sensing signals are exposed to both power-based and feature-based detection techniques. These advanced intercept threats make it difficult to maintain sensing security through traditional waveform design or power control alone, and necessitate new approaches that address both signal power and feature observability.

A. Properties of Intercepted Signals

To evaluate the sensing security performance, the power and cyclostationary behavior of the received signals should be analyzed. Based on the received signal (4), we define $\mathbf{r} = [r_1, \dots, r_K]^T \in \mathbb{C}^K$ as the signals received by the advanced ER aircraft across all the K subcarriers. The power collected by the advanced ER aircraft across K subcarriers can be directly given by

$$P_E = \mathbb{E} \left\{ \|\mathbf{r}\|_F^2 \right\} = \sum_{k=1}^K \|\alpha_k \mathbf{a}_t^H(\theta_E, f_k) \mathbf{F}_{\text{RF}} \mathbf{F}_k\|_F^2 + K\sigma_E^2. \quad (5)$$

To further study the cyclostationary property, the signals are converted into the frequency domain by the K -point FFTs, which can be expressed as

$$\widehat{\mathbf{r}} = \text{FFT}(\mathbf{r}) = \mathbf{V}_{\text{FFT}} \mathbf{r} \in \mathbb{C}^K, \quad (6)$$

where $\mathbf{V}_{\text{FFT}} \in \mathbb{C}^{K \times K}$ denotes the FFT matrix defined by

$$\mathbf{V}_{\text{FFT}}[i, j] = \exp\left(-j \frac{2\pi}{K} (i-1)(j-1)\right), i, j \in [1, K]. \quad (7)$$

Based on the frequency-domain signal (6), we can derive its corresponding cyclic spectrum [43] by

$$\mathbf{C}_E(m, n) = \frac{1}{W} \sum_{w=-\frac{W}{2}}^{\frac{W}{2}-1} \widehat{\mathbf{r}}\left(m + \frac{n}{2} + w\right) \widehat{\mathbf{r}}^*\left(m - \frac{n}{2} + w\right), \quad (8)$$

$m \in \mathcal{M}, n \in \mathcal{N}$,

where W denotes the length of analysis window of the advanced ER aircraft, and $\mathcal{M} = \{0, 1, 2, \dots, K-W\}$ and $\mathcal{N} = \{0, 2, 4, \dots, K-W\}$. Besides, we define the cyclic frequency and frequency as $\alpha = n f_s$ and $f = m f_s$, respectively, with the sampling frequency f_s .

Substituting (6) into (8), we can further rewrite the cyclic spectrum of the received signal as

$$\mathbf{C}_E(m, n) = \frac{1}{W} \text{Tr} \left\{ \mathbf{\Lambda}_{m,n} \widehat{\mathbf{r}} \widehat{\mathbf{r}}^H \right\}, m \in \mathcal{M}, n \in \mathcal{N}, \quad (9)$$

where we define

$$\mathbf{\Lambda}_{m,n}[i, j] = \begin{cases} 1, & i - j = n, m \leq i < m + W \\ 0, & \text{otherwise} \end{cases}, \forall i, j.$$

Note that the cyclic spectrum \mathbf{C}_E exhibits randomness due to the randomness of the received signal (9). To have a better analysis of the characteristics of the cyclic spectrum, we give the following definition.

Definition 1. (*Ergodic Cyclic Spectrum*): To analyze the characteristics of the random cyclic spectrum (9), we introduce an ergodic cyclic spectrum, $\tilde{\mathbf{C}}_E$, which is defined by

$$\tilde{\mathbf{C}}_E(m, n) = \mathbb{E} \left\{ \mathbf{C}_E(m, n) \right\}, m \in \mathcal{M}, n \in \mathcal{N}. \quad (10)$$

Based on (9), we notice that $\mathbf{\Lambda}_{m,n}, m \in \mathcal{M}, n \in \mathcal{N}$ are deterministic and $\widehat{\mathbf{r}}$ is random. To this end, the ergodic cyclic spectrum (10) can be further rewritten as

$$\tilde{\mathbf{C}}_E(m, n) = \frac{1}{W} \text{Tr} \left\{ \mathbf{\Lambda}_{m,n} \mathbb{E} \left\{ \widehat{\mathbf{r}} \widehat{\mathbf{r}}^H \right\} \right\}, m \in \mathcal{M}, n \in \mathcal{N}. \quad (11)$$

Based on **Definition 1**, the ergodic cyclic spectrum of the received signal can be expressed by

$$\tilde{\mathbf{C}}_E(m, n) = \frac{1}{W} \text{Tr} \left\{ \mathbf{\Lambda}_{m,n} \left(\mathbf{V}_{\text{FFT}} (\mathbf{\Xi} + \mathbf{\Omega}) \mathbf{V}_{\text{FFT}}^H \right) \right\}, \quad (12)$$

where we define $\mathbf{\Xi} = \text{Diag}(|\alpha_1|^2 \|\mathbf{a}_t^H(\theta_E, f_1) \mathbf{F}_{\text{RF}} \mathbf{F}_1\|_F^2, \dots, |\alpha_K|^2 \|\mathbf{a}_t^H(\theta_E, f_K) \mathbf{F}_{\text{RF}} \mathbf{F}_K\|_F^2) \in \mathbb{C}^{K \times K}$ and $\mathbf{\Omega} = \text{Diag}(\sigma_E^2, \dots, \sigma_E^2) \in \mathbb{C}^{K \times K}$.

B. LPI Design Guideline

With the properties of intercepted signals at hand, an effective LPI design guideline should be established. Since the advanced ER aircraft applies both PD and CA intercept processing methods to determine the existence of the received signal, the probability of intercept, Pr_{int} , is related to the power (5) and the ergodic cyclic spectrum (12) of the received signal. To this end, we can write Pr_{int} as a function about P_E and $\tilde{\mathbf{C}}_E$ as follows.

$$\text{Pr}_{\text{int}} = \mathcal{F}(P_E, \tilde{\mathbf{C}}_E), \quad (13)$$

where the specific form of the function $\mathcal{F}(\cdot)$ is determined by the internal decision-making mechanisms of the advanced ER aircraft, which is unknown at the BS.

Although the knowledge of the function $\mathcal{F}(\cdot)$ is not available, we can build some useful relationships between the probability of intercept and properties of intercepted signals.

1) *Anti-PD Design Guideline*: To combat PD, a direct and effective approach is to guarantee the received power (5) as low as possible so that the preset threshold cannot be reached.

2) *Anti-CA Design Guideline*: To combat CA, an effective heuristic approach is to enforce the ergodic cyclic spectrum of the received signals close to that of the AWGN so that the ISAC signal can be hidden in the environmental noise. Due to this, the ergodic cyclic spectrum of the AWGN can be expressed as

$$\tilde{\mathbf{C}}_N(m, n) = \frac{1}{W} \text{Tr} \left\{ \mathbf{\Lambda}_{m,n} \left(\mathbf{V}_{\text{FFT}} \mathbf{\Omega}_0 \mathbf{V}_{\text{FFT}}^H \right) \right\}, \quad (14)$$

where $\mathbf{\Omega}_0 = \text{Diag}(\sigma_0^2, \dots, \sigma_0^2) \in \mathbb{C}^{K \times K}$ denotes the corresponding diagonal form of the general AWGN, and σ_0^2 denotes the power spectral density. To better analyze the ergodic cyclic

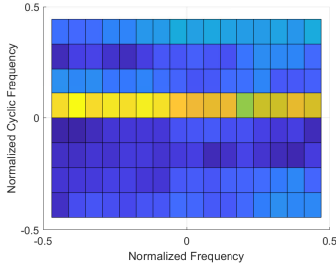


Fig. 2. Cyclic spectrum of the AWGN.

spectrum (14), we equivalently rewrite it to a more intuitive form as follows.

$$\begin{cases} \tilde{\mathbf{C}}_N(m, n) = N_0, & n = 0 \\ \tilde{\mathbf{C}}_N(m, n) = 0, & n \neq 0 \end{cases}, \quad (15)$$

where N_0 represents a constant power spectral density after processing. For visualization, the cyclic spectrum of the AWGN is presented in Fig. 2. Based on (15) and Fig.2, we notice that the AWGN does not exhibit any cyclostationary properties [43].

To enforce the ergodic cyclic spectrum of the received signal (12) approaching that of the AWGN (14), we give the following insight to specify the anti-CA design objective.

Insight 1. (Anti-CA Design Objective): *It can be noticed that the only difference between the ergodic cyclic spectrum of the received signal and the AWGN is the term $(\Xi + \Omega)$ and the term Ω_0 , which are both diagonal matrices. Since the diagonal elements of Ω_0 are equal, the ergodic cyclic spectrum of the AWGN stays constant in the frequency domain. Based on this, an effective approach to assimilate $\tilde{\mathbf{C}}_E$ with $\tilde{\mathbf{C}}_N$ for anti-CA design is to force the diagonal elements of Ξ to be equal.*

Remark 1. (Design Guideline Merits): *The state-of-the-art literature [37], [44], [45] has also approximated the cyclic spectrum characteristic of the designed waveform to the AWGN. These works [37], [44], [45] are based on optimizing certain explicit features of the cyclic spectrum, i.e., mean square error (MSE) relative to AWGN or cyclic frequency side-lobe level (CFSL), but these metrics are inherently incomplete descriptors and do not fully characterize the global structural properties of the cyclic spectrum. Our approach addresses this limitation by exploiting the intrinsic mathematical properties of the cyclic spectrum matrix itself.*

IV. SENSING SECURITY ORIENTED OFDM-ISAC PROBLEM FORMULATION

In this section, we first derive the performance metrics, and then formulate the design problem.

A. Performance Metrics

In this work, we aim to achieve sensing security in the considered ISAC system.

For communication performance, based on (2), the achievable data rate for the u -th user at the k -th subcarrier is

$$R_{k,u}(\mathbf{F}_{\text{RF}}, \mathbf{F}_k) = \log_2(1 + \text{SINR}_{k,u}(\mathbf{F}_{\text{RF}}, \mathbf{F}_k)), \quad (16)$$

with the signal-to-interference-plus-noise ratio (SINR) of the received signal

$$\text{SINR}_{k,u}(\mathbf{F}_{\text{RF}}, \mathbf{F}_k) = \frac{|\mathbf{h}_{k,u}^H \mathbf{F}_{\text{RF}} \mathbf{f}_{k,u}|^2}{\sum_{i \neq u} |\mathbf{h}_{k,u}^H \mathbf{F}_{\text{RF}} \mathbf{f}_{k,i}|^2 + \sigma_C^2}. \quad (17)$$

For radar performance, based on (3), the output radar signal-to-noise ratio (SNR) can be expressed as

$$\gamma(\{\mathbf{w}_k\}, \mathbf{F}_{\text{RF}}, \{\mathbf{F}_k\}) = \chi \sum_{k=1}^K \|\mathbf{w}_k^H \mathbf{A}(\theta_E, f_k) \mathbf{F}_{\text{RF}} \mathbf{F}_k\|_F^2, \quad (18)$$

where we define $\chi = |\zeta_E|^2 / (\sigma_R^2 \sum_{k=1}^K P_{R,k})$, with the power budget $P_{R,k} = \|\mathbf{w}_k\|_F^2, \forall k$.

Note that the radar detector aims to determine the existence of the ER aircraft. According to [46], the probability of detection can be written as

$$\text{Pr}_d = \mathcal{Q}\left(\sqrt{2\gamma(\{\mathbf{w}_k\}, \mathbf{F}_{\text{RF}}, \{\mathbf{F}_k\})}, \sqrt{-\ln(\text{Pr}_{\text{fa}})}\right), \quad (19)$$

where Pr_{fa} denotes the probability of false alarm and $\mathcal{Q}(\cdot, \cdot)$ denotes the Marcum Q function of order 1. Based on this, we give the following remark to characterize the sensing performance of the ISAC-OFDM system.

Remark 2. (Sensing Design Metric Equivalence): *According to the detection probability (19), for a given false alarm probability, the detection probability is monotonically increasing with the radar SNR. Therefore, for a required probability of false alarm, increasing the probability of detection is equivalent to increasing the radar SNR.*

When it comes to sensing security performance, we follow the LPI design guideline in Sec. III-B.

B. Problem Statement

Since the exact location information of the target is hard to obtain in practice, we assume that the angular location of the target is roughly known within the interval $[\theta_0 - \Delta\theta, \theta_0 + \Delta\theta]$. Then, we divide the angle interval into a discrete set, i.e., $\Theta = \{\theta_q\}_{q=1}^Q$, where Q denotes the number of discrete points in the angle interval.

To achieve LPI against multiple threats, i.e., PD and CA, for the considered OFDM-ISAC system, we propose to jointly design the radar filter, $\{\mathbf{w}_k\}$, analog beamformer, \mathbf{F}_{RF} , and digital beamformer, $\{\mathbf{F}_k\}$, by minimizing the probability of intercept while meeting the requirements of radar detection, communication QoS, power and hardware. Mathematically, the LPI design problem can be formulated as

$$\min_{\{\mathbf{w}_k\}, \mathbf{F}_{\text{RF}}, \{\mathbf{F}_k\}} \max_q \text{Pr}_{\text{int},q}, \quad (20a)$$

$$\text{s.t.} \quad \gamma_q(\{\mathbf{w}_k\}, \mathbf{F}_{\text{RF}}, \{\mathbf{F}_k\}) \geq \Gamma, \forall q, \quad (20b)$$

$$R_{k,u}(\mathbf{F}_{\text{RF}}, \{\mathbf{F}_k\}) \geq \xi_{k,u}, \forall k, u, \quad (20c)$$

$$\|\mathbf{F}_{\text{RF}} \mathbf{F}_k\|_F^2 \leq P_{T,k}, \forall k, \quad (20d)$$

$$|\mathbf{F}_{\text{RF}}[i, j]| = 1, \forall i, j, \quad (20e)$$

$$\|\mathbf{w}_k\|_F^2 = P_{R,k}, \forall k, \quad (20f)$$

where Γ denotes the output radar SNR threshold, $\xi_{k,u}$ denotes the communication QoS requirement for the u -th user at the k -th subcarrier, $P_{T,k}$ and $P_{R,k}$ denotes the power budgets for the transmitter and receiver, respectively, and the constraint (20e) denotes the hardware constraint for the analog beamformer.

Note that the LPI design problem (20) is a non-convex optimization problem with an uncertain complicated objective function, constant modulus constraint, and coupling among variables. To tackle these difficulties, we propose an iterative approach to efficiently solve this problem in the following sections.

V. LPI DESIGN AGAINST MULTI-INTERCEPT THREATS

In this section, we first reformulate the original problem into a more tractable form, and then propose an effective solver to jointly design the radar filter and hybrid transmitter.

A. Reformulation of Objective Function

It is noticed that the objective function (20a) involves a function $\mathcal{F}(\cdot)$. In the practical scenario, the specific information of the function $\mathcal{F}(\cdot)$ tends to be unknown by the OFDM-ISAC BS, which makes the original problem extremely tricky. To address this issue, we aim to transform the objective function (20a) into a more tractable form.

1) *Specification of Anti-PD Design*: Based on the anti-PD design guideline in Sec. III-B, the power of the received signals should be suppressed, leading to the following problem of LPI design against PD:

$$\min_{\mathbf{F}_{\text{RF}}, \{\mathbf{F}_k\}} \max_q \sum_{k=1}^K \|\alpha_k \mathbf{a}_t^H(\theta_q, f_k) \mathbf{F}_{\text{RF}} \mathbf{F}_k\|_F^2. \quad (21)$$

2) *Specification of Anti-CA Design*: Based on the anti-CA design guideline in **Insight 1**, the diagonal elements of Ξ should be identical, leading to the following problem of LPI design against CA

$$\text{Find}_{\mathbf{F}_{\text{RF}}, \{\mathbf{F}_k\}} |\alpha_k|^2 \|\mathbf{a}_t^H(\theta_q, f_k) \mathbf{F}_{\text{RF}} \mathbf{F}_k\|_F^2 = C_q, \forall k, \quad (22)$$

where $C_q, \forall q$ represents a constant value.

Now, based on the specification of anti-PD&CA design, we consider problems (21) and (22) together, the original LPI design problem (20) can be reformulated as

$$\min_{\mathbf{F}_{\text{RF}}, \{\mathbf{F}_k\}, \{\mathbf{w}_k\}} \tau, \quad (23a)$$

$$\text{s.t.} \quad |\alpha_k|^2 \|\mathbf{a}_t^H(\theta_q, f_k) \mathbf{F}_{\text{RF}} \mathbf{F}_k\|_F^2 = \tau, \forall k, q, \quad (23b)$$

$$(20b) - (20f), \quad (23c)$$

where τ represents an introduced auxiliary variable.

B. Receive Filter Design

We notice that the receive filter $\{\mathbf{w}_k\}$ only exists in the constraint (20b), so the receive filter is optimized by solving:

$$\max_{\{\mathbf{w}_k\}} \min_q \gamma_q(\{\mathbf{w}_k\}, \mathbf{F}_{\text{RF}}, \{\mathbf{F}_k\}), \text{ s.t. } \|\mathbf{w}_k\|_F^2 = P_{R,k}, \forall k, \quad (24)$$

which is a maximization-minimization non-convex problem. To decouple variables in the objective functions and constraints, we introduce several auxiliary variables, t and $\{\mathbf{u}_{k,q}\}$, transforming the problem (24) into a more tractable form:

$$\min_{t, \{\mathbf{w}_k\}, \{\mathbf{u}_{k,q}\}} -t, \quad (25a)$$

$$\text{s.t.} \quad \sum_{k=1}^K \|\mathbf{u}_{k,q}\|_F^2 \geq t, \forall q, \quad (25b)$$

$$\|\mathbf{w}_k\|_F^2 = P_{R,k}, \forall k, \quad (25c)$$

$$\mathbf{u}_{k,q} = \mathbf{F}_k^H \mathbf{F}_{\text{RF}}^H \mathbf{A}^H(\theta_q, f_k) \mathbf{w}_k, \forall q, k, \quad (25d)$$

$$t \geq 0. \quad (25e)$$

The associated augmented Lagrange (AL) function via penalizing the equality constraint (25d) is given by

$$\begin{aligned} \mathcal{L}_R(t, \{\mathbf{w}_k\}, \{\mathbf{u}_{k,q}\}, \{\boldsymbol{\nu}_{k,q}\}) = & -t \\ & + \frac{\mu}{2} \sum_{q=1}^Q \sum_{k=1}^K \|\mathbf{u}_{k,q} - \mathbf{F}_k^H \mathbf{F}_{\text{RF}}^H \mathbf{A}^H(\theta_q, f_k) \mathbf{w}_k + \boldsymbol{\nu}_{k,q}\|_F^2, \end{aligned}$$

where $\{\boldsymbol{\nu}_{k,q}\}$ is dual variable for the constraint (25d) and $\mu > 0$ is the corresponding penalty parameter. Then, the receive filter can be optimized by solving the following subproblems.

1) *Update of $t, \{\mathbf{u}_{k,q}\}$* : With other variables fixed, $t, \{\mathbf{u}_{k,q}\}$ can be updated by solving the subproblem:

$$\min_{t, \{\mathbf{u}_{k,q}\}} -t + \frac{\mu}{2} \sum_{q=1}^Q \sum_{k=1}^K \|\mathbf{u}_{k,q} - \tilde{\boldsymbol{\nu}}_{k,q}\|_F^2, \quad (26)$$

$$\text{s.t.} \quad \sum_{k=1}^K \|\mathbf{u}_{k,q}\|_F^2 \geq t, \forall q,$$

where $\tilde{\boldsymbol{\nu}}_{k,q} = \mathbf{F}_k^H \mathbf{F}_{\text{RF}}^H \mathbf{A}^H(\theta_q, f_k) \mathbf{w}_k - \boldsymbol{\nu}_{k,q}, \forall k, q$. The following lemma provides solutions to the subproblem (26).

Lemma 1. *Problem (26) is a joint quadratic program with a parameterized constraint (JQP-PC), whose close-form solution can be found in two steps.*

• *Step 1: Fix $t, \mathbf{u}_{k,q}$ is updated by*

$$\mathbf{u}_{k,q} = \begin{cases} \tilde{\boldsymbol{\nu}}_{k,q} & , \|\tilde{\boldsymbol{\nu}}_{k,q}\|_F^2 \geq t \\ t^{1/2} \frac{\tilde{\boldsymbol{\nu}}_{k,q}}{\|\tilde{\boldsymbol{\nu}}_{k,q}\|_F} & , \text{otherwise} \end{cases}, \quad (27)$$

where $\tilde{\mathbf{V}}_q = [\tilde{\boldsymbol{\nu}}_{1,q}, \dots, \tilde{\boldsymbol{\nu}}_{K,q}]$.

• *Step 2: Fix $\mathbf{u}_{k,q}, t$ is updated by solving*

$$\frac{\mu}{2} \sum_{q=1}^Q \sum_{k=1}^K \beta_q \left(1 - t^{-1/2} \|\tilde{\mathbf{V}}_q\|_F\right) = 1, \quad (28)$$

with *Newton's or bisection method*, where $\beta_q = 0$ if $\|\tilde{\mathbf{V}}_q\|_F^2 \geq t$; otherwise, $\beta_q = 0$.

Proof: Please refer to Appendix A. ■

2) *Update of $\{\mathbf{w}_k\}$* : With other variables fixed, \mathbf{w}_k can be updated by solving the subproblem:

$$\min_{\mathbf{w}_k} \sum_{q=1}^Q \|\mathbf{u}_{k,q} - \mathbf{F}_k^H \mathbf{F}_{\text{RF}}^H \mathbf{A}^H(\theta_q, f_k) \mathbf{w}_k + \boldsymbol{\nu}_{k,q}\|_F^2, \quad (29)$$

$$\text{s.t.} \quad \|\mathbf{w}_k\|_F^2 = P_{R,k}.$$

The following lemma provides solutions to the subproblem (29).

Lemma 2. *Problem (29) is a quadratically constrained quadratic program (QCQP) with one constraint (QCQP-1), whose close-form solution can be derived as*

$$\mathbf{w}_k(\kappa_k) = \left(\tilde{\mathbf{G}}_k + \kappa_k \mathbf{I}_{M_t} \right)^{-1} \tilde{\Phi}_k, \quad (30)$$

where $\tilde{\mathbf{G}}_k$ and $\tilde{\Phi}_k$ are defined in Appendix B, and κ_k can be obtained by solving

$$\sum_{n=1}^{M_r} \frac{[\tilde{\mathbf{G}}_k^H \tilde{\Phi}_k \tilde{\Phi}_k^H \tilde{\mathbf{G}}_k]_{n,n}}{(\kappa_k + [\tilde{\Sigma}_k]_{n,n})^2} = P_{R,k}, \quad (31)$$

using Newton's or bisection method, where $\tilde{\mathbf{G}}_k$ and $\tilde{\Sigma}_k$ are defined in Appendix B.

Proof: Please refer to Appendix B. ■

3) *Update of $\nu_{k,q}$:* With other variables fixed, $\nu_{k,q}$ can be updated by

$$\nu_{k,q}^{[l+1]} = \mathbf{u}_{k,q}^{[l+1]} - \mathbf{F}_k^H \mathbf{F}_{\text{RF}}^H \mathbf{A}^H(\theta_q, f_k) \mathbf{w}_k^{[l+1]} + \nu_{k,q}^{[l]}, \quad (32)$$

where $(\cdot)^{[l+1]}$ is the next iteration point of $(\cdot)^{[l]}$.

C. Hybrid Transmitter Design

To decouple the hybrid digital and analog beamformers and the constraints (23a), (20b)-(20f), we introduce several auxiliary variables $\{\{\mathbf{T}_k\}, \{\mathbf{b}_{k,q}\}, \{\mathbf{z}_{k,q}\}, \{Y_{k,u}^{k,i}\}\}$ to rewrite the problem (23) as

$$\min_{\mathbf{F}_{\text{RF}}, \{\mathbf{F}_k\}, \{\mathbf{T}_k\}, \tau, \{\mathbf{b}_{k,q}\}, \{\mathbf{z}_{k,q}\}, \{Y_{k,u}^{k,i}\}} \tau, \quad (33a)$$

$$\text{s.t. } |\alpha_k|^2 \|\mathbf{b}_{k,q}\|_F^2 = \tau, \forall k, q, \quad (33b)$$

$$\chi \sum_{k=1}^K \|\mathbf{z}_{k,q}\|_F^2 \geq \Gamma, \forall q, \quad (33c)$$

$$\frac{|Y_{k,u}^{k,u}|^2}{\sum_{i \neq u}^U |Y_{k,u}^{k,i}|^2 + \sigma_C^2} \geq 2^{\xi_{k,u}} - 1, \forall k, u, \quad (33d)$$

$$\|\mathbf{T}_k\|_F^2 = \mathcal{P}_{T,k}, \forall k, \quad (33e)$$

$$|\mathbf{F}_{\text{RF}}[i, j]| = 1, \forall i, j, \quad (33f)$$

$$\mathbf{T}_k = \mathbf{F}_{\text{RF}} \mathbf{F}_k, \forall k, \quad (33g)$$

$$\mathbf{b}_{k,q} = \mathbf{T}_k^H \mathbf{a}_t(\theta_q, f_k), \forall k, q, \quad (33h)$$

$$\mathbf{z}_{k,q} = \mathbf{T}_k^H \mathbf{A}^H(\theta_q, f_k) \mathbf{w}_k, \forall k, q, \quad (33i)$$

$$Y_{k,u}^{k,i} = \mathbf{h}_{k,u}^H \mathbf{t}_{k,i}, \forall k, u, i, \quad (33j)$$

$$\tau \geq 0, \quad (33k)$$

whose associated AL function via penalizing the equality constraints (33g)-(33j) is given in (34), where $\{\mathbf{D}_k\}, \{\mathbf{v}_{k,q}\}, \{\mathbf{m}_{k,q}\}, \{Q_{k,u}^{k,i}\}$ and $\rho_1, \rho_2, \rho_3, \rho_4 > 0$ are dual variables and corresponding penalty parameters, respectively. Now, the problem (33) can be iteratively solved as follows.

1) *Update of $\{\mathbf{T}_k\}$:* With other variables fixed, \mathbf{T}_k can be updated by solving

$$\begin{aligned} \min_{\mathbf{T}_k} & \frac{\rho_1}{2} \|\mathbf{T}_k - \mathbf{F}_{\text{RF}} \mathbf{F}_k + \mathbf{D}_k\|_F^2 \\ & + \frac{\rho_2}{2} \sum_{q=1}^Q \|\mathbf{b}_{k,q} - \mathbf{T}_k^H \mathbf{a}_t(\theta_q, f_k) + \mathbf{v}_{k,q}\|_F^2 \\ & + \frac{\rho_3}{2} \sum_{q=1}^Q \|\mathbf{z}_{k,q} - \mathbf{T}_k^H \mathbf{A}^H(\theta_q, f_k) \mathbf{w}_k + \mathbf{m}_{k,q}\|_F^2 \\ & + \frac{\rho_4}{2} \sum_{u=1}^U \sum_{i=1}^U \left\| Y_{k,u}^{k,i} - \mathbf{h}_{k,u}^H \mathbf{t}_{k,i} + Q_{k,u}^{k,i} \right\|_F^2, \quad (35) \\ \text{s.t. } & \|\mathbf{T}_k\|_F^2 = \mathcal{P}_{T,k}, \forall k. \end{aligned}$$

which is also a convex QCQP-1 whose optimal solutions can be obtained by analyzing the KKT conditions like the problem (29) in Appendix B.

2) *Update of $\tau, \{\mathbf{b}_{k,q}\}$:* With other variables fixed, $\tau, \{\mathbf{b}_{k,q}\}$ can be updated by solving

$$\begin{aligned} \min_{\tau, \{\mathbf{b}_{k,q}\}} & \tau + \frac{\rho_2}{2} \sum_{k=1}^K \sum_{q=1}^Q \|\mathbf{b}_{k,q} - \tilde{\mathbf{v}}_{k,q}\|_F^2, \quad (36) \\ \text{s.t. } & \|\mathbf{b}_{k,q}\|_F^2 = \frac{\tau}{|\alpha_k|^2}, \forall k, q, \end{aligned}$$

where $\tilde{\mathbf{v}}_{k,q} = \mathbf{T}_k^H \mathbf{a}_t(\theta_q, f_k) - \mathbf{v}_{k,q}, \forall k, q$. Note that this problem is also a JQP-PC which can be solved like the problem (26) in Appendix A.

3) *Update of $\{\mathbf{z}_{k,q}\}$:* With other variables fixed, $\{\mathbf{z}_{k,q}\}$ can be updated by solving

$$\min_{\{\mathbf{z}_{k,q}\}} \sum_{k=1}^K \|\mathbf{z}_{k,q} - \tilde{\mathbf{m}}_{k,q}\|_F^2, \text{ s.t. } \sum_{k=1}^K \|\mathbf{z}_{k,q}\|_F^2 \geq \frac{\Gamma}{\gamma}, \quad (37)$$

where $\tilde{\mathbf{m}}_{k,q} = \mathbf{T}_k^H \mathbf{G}^H(\theta_q, f_k) \mathbf{w}_k - \mathbf{m}_{k,q}, \forall k, q$. The subproblem (37) can be equivalently rewritten as

$$\min_{\hat{\mathbf{z}}_q} \|\hat{\mathbf{z}}_q - \hat{\mathbf{m}}_q\|_F^2, \text{ s.t. } \|\hat{\mathbf{z}}_q\|_F^2 \geq \frac{\Gamma}{\gamma}, \quad (38)$$

where $\hat{\mathbf{z}}_q = [\mathbf{z}_{1,q}^T, \dots, \mathbf{z}_{K,q}^T]^T \in \mathbb{C}^{UK}$, $\hat{\mathbf{m}}_q = [\tilde{\mathbf{m}}_{1,q}^T, \dots, \tilde{\mathbf{m}}_{K,q}^T]^T \in \mathbb{C}^{UK}$. This problem is also a convex QCQP-1 whose optimal solutions can be obtained by analyzing the KKT conditions similar to the problem (29) in Appendix B.

4) *Update of $\{Y_{k,u}^{k,i}\}$:* With other variables fixed, $\{Y_{k,u}^{k,i}\}$ can be updated by solving

$$\begin{aligned} \min_{\{Y_{k,u}^{k,i}\}} & \sum_{i=1}^U \left\| Y_{k,u}^{k,i} - \mathbf{h}_{k,u}^H \mathbf{t}_{k,i} + Q_{k,u}^{k,i} \right\|_F^2, \\ \text{s.t. } & (2^{\xi_{k,u}} - 1) \sum_{i \neq u}^U |Y_{k,u}^{k,i}|^2 - |Y_{k,u}^{k,u}|^2 + (2^{\xi_{k,u}} - 1) \sigma_C^2 \leq 0, \quad (39) \end{aligned}$$

which is also a QCQP-1 whose optimal solutions can be obtained by applying the KKT conditions similar to the problem (29) in Appendix B.

$$\begin{aligned}
& \mathcal{L}_T \left(\mathbf{F}_{\text{RF}}, \{\mathbf{F}_k\}, \{\mathbf{T}_k\}, \tau, \{\mathbf{b}_{k,q}\}, \{\mathbf{z}_{k,q}\}, \{Y_{k,u}^{k,i}\}, \{\mathbf{D}_k\}, \{\mathbf{v}_{k,q}\}, \{\mathbf{m}_{k,q}\}, \{Q_{k,u}^{k,i}\} \right) \\
&= \tau + \frac{\rho_1}{2} \sum_{k=1}^K \|\mathbf{T}_k - \mathbf{F}_{\text{RF}} \mathbf{F}_k + \mathbf{D}_k\|_F^2 + \frac{\rho_2}{2} \sum_{k=1}^K \sum_{q=1}^Q \|\mathbf{b}_{k,q} - \mathbf{T}_k^H \mathbf{a}_t(\theta_q, f_k) + \mathbf{v}_{k,q}\|_F^2 \\
&+ \frac{\rho_3}{2} \sum_{k=1}^K \sum_{q=1}^Q \|\mathbf{z}_{k,q} - \mathbf{T}_k^H \mathbf{A}^H(\theta_q, f_k) \mathbf{w}_k + \mathbf{m}_{k,q}\|_F^2 + \frac{\rho_4}{2} \sum_{k=1}^K \sum_{u=1}^U \sum_{i=1}^U \left\| Y_{k,u}^{k,i} - \mathbf{h}_{k,u}^H \mathbf{t}_{k,i} + Q_{k,u}^{k,i} \right\|_F^2,
\end{aligned} \tag{34}$$

5) *Update of $\{\mathbf{F}_k\}$* : With other variables fixed, \mathbf{F}_k can be updated by solving an unconstrained subproblem

$$\min_{\mathbf{F}_k} \|\mathbf{Z}_k - \mathbf{F}_{\text{RF}} \mathbf{F}_k\|_F^2, \tag{40}$$

where $\mathbf{Z}_k = \mathbf{T}_k + \mathbf{D}_k, \forall k$. Taking the first-order optimality condition, its solution can be directly derived by

$$\mathbf{F}_k = (\mathbf{F}_{\text{RF}}^H \mathbf{F}_{\text{RF}})^{-1} \mathbf{F}_{\text{RF}}^H \mathbf{Z}_k. \tag{41}$$

6) *Update of \mathbf{F}_{RF}* : With other variables fixed, \mathbf{F}_{RF} can be updated by solving

$$\min_{\mathbf{F}_{\text{RF}}} \sum_{k=1}^K \|\mathbf{Z}_k - \mathbf{F}_{\text{RF}} \mathbf{F}_k\|_F^2, \text{ s.t. } |\mathbf{F}_{\text{RF}}[i, j]| = 1, \forall i, j. \tag{42}$$

This subproblem is hard to solve due to the discrete constraint involved in the constant modulus hardware requirement. To tackle this difficulty, we rewrite the constant modulus constraint into an equivalent form:

$$\mathbf{F}_{\text{RF}}[i, j] = \exp(-j\vartheta_{i,j}), \vartheta_{i,j} \in (0, 2\pi]. \tag{43}$$

The constraint (43) indicates that the elements of \mathbf{F}_{RF} lie on a closed unit circle, which is a closed convex set. Therefore, the subproblem (42) can be solved under a cyclic coordinate descent (CCD) framework [47].

7) *Update of $\{\mathbf{D}_k\}, \{\mathbf{v}_{k,q}\}, \{\mathbf{m}_{k,q}\}, \{Q_{k,u}^{k,i}\}$* : With other variables fixed, the dual variables can be updated by

$$\mathbf{D}_k^{[r+1]} = \mathbf{T}_k^{[r+1]} - \mathbf{F}_{\text{RF}}^{[r+1]} \mathbf{F}_k^{[r+1]} + \mathbf{D}_k^{[r]}, \tag{44a}$$

$$\mathbf{v}_{k,q}^{[r+1]} = \mathbf{b}_{k,q}^{[r+1]} - (\mathbf{T}_k^{[r+1]})^H \mathbf{a}_t(\theta_q, f_k) + \mathbf{v}_{k,q}^{[r]}, \tag{44b}$$

$$\mathbf{m}_{k,q}^{[r+1]} = \mathbf{z}_{k,q}^{[r+1]} - (\mathbf{T}_k^{[r+1]})^H \mathbf{A}^H(\theta_q, f_k) \mathbf{w}_k + \mathbf{m}_{k,q}^{[r]}, \tag{44c}$$

$$Q_{k,u}^{k,i[r+1]} = Y_{k,u}^{k,i[r+1]} - p_{k,u} \mathbf{h}_{k,u}^H \mathbf{t}_{k,i}^{[r+1]} + Q_{k,u}^{k,i[r]}. \tag{44d}$$

D. Summary

According to the derivations above, we summarize the proposed algorithm for the anti-PD&CA LPI design for secure OFDM-ISAC systems in **Algorithm 1**.

Then, we analyze the computational complexity of the proposed algorithm. There are two inner loops and one outer loop in **Algorithm 1**. 1) The first inner loop updating the receive filter: updating $(t, \{\mathbf{u}_{k,q}\})$ needs the complexity of $\mathcal{O}(QKU)$ and updating $\{\mathbf{w}_k\}$ needs the complexity of $\mathcal{O}(KM_r^2)$. 2) The second inner loop updating the hybrid beamformer: updating $\{\mathbf{T}_k\}$ needs the complexity of $\mathcal{O}(KM_t^3)$, updating $(\tau, \{\mathbf{b}_{k,q}\})$ needs the complexity of $\mathcal{O}(QKU)$, updating $\{\mathbf{z}_{k,q}\}$ needs the complexity of $\mathcal{O}(QKU)$, and updating $\{Y_{k,u}^{k,i}\}$ needs the

Algorithm 1: Sensing Security Oriented ISAC Design

Input: System parameters, $\{\mathbf{h}_{k,u}\}, I_1, I_2$.

Output: $\{\mathbf{w}_k\}, \mathbf{F}_{\text{RF}}, \{\mathbf{F}_k\}$.

```

1 Initialize:  $\{\mathbf{w}_k^0\}, \mathbf{F}_{\text{RF}}^0, \{\mathbf{F}_k^0\}, i = 0;$ 
2 while No Convergence do
3    $i = i + 1;$ 
4   for  $l = 0, \dots, I_1 - 1$  do
5     Update  $\{\mathbf{u}_{k,q}^{[l+1]}\}$  by (27), and update  $t^{[l+1]}$  by
       solving (28).
6     Update  $\{\mathbf{w}_k^{[l+1]}\}$  by (30).
7     Update dual variable by (32).
8   end
9   Set  $\{\mathbf{w}_k^i\} = \{\mathbf{w}_k^{[l+1]}\}$ .
10  for  $r = 0, \dots, I_2 - 1$  do
11    Update  $\{\mathbf{T}_k^{[r+1]}\}$  by solving (35).
12    Update  $\{\mathbf{b}_{k,q}^{[r+1]}\}$  and update  $\tau^{[r+1]}$  by solving
       (36).
13    Update  $\{\mathbf{z}_{k,q}^{[r+1]}\}$  by solving (37).
14    Update  $\{Y_{k,u}^{k,i[r+1]}\}$  by solving (39).
15    Update  $\{\mathbf{F}_k^{[r+1]}\}$  by (41).
16    Update  $\mathbf{F}_{\text{RF}}^{[r+1]}$  by (42) under CCD framework.
17    Update dual variables by (44).
18  end
19  Set  $\{\mathbf{F}_k^i\} = \{\mathbf{F}_k^{[r+1]}\}$  and  $\mathbf{F}_{\text{RF}}^i = \mathbf{F}_{\text{RF}}^{[r+1]}$ .
20 end
21  $\{\mathbf{w}_k\} = \{\mathbf{w}_k^i\}, \{\mathbf{F}_k\} = \{\mathbf{F}_k^i\}$  and  $\mathbf{F}_{\text{RF}} = \mathbf{F}_{\text{RF}}^i$ .

```

complexity of $\mathcal{O}(KU^2)$. Besides, updating $\{\mathbf{F}_k\}$ needs the complexity of $\mathcal{O}(N_{\text{RF}}^3)$, and updating \mathbf{F}_{RF} needs the complexity of $\mathcal{O}(I_{\text{CCD}} KM_t N_{\text{RF}}^2 U)$, where I_{CCD} denotes the iteration number in the CCD framework. To sum up, the total complexity is $\mathcal{O}(I_O(I_1(QKU + KM_r^2) + I_2(KM_t^3 + QKU + KU^2 + N_{\text{RF}}^3 + I_{\text{CCD}} KM_t N_{\text{RF}}^2 U)))$, where I_1 and I_2 denotes the iteration number for the first and second inner loops, respectively, and I_O denotes the iteration number for the outer loop.

VI. NUMERICAL SIMULATIONS

In this section, we provide numerical simulations to evaluate the performance of the proposed LPI design for the secure OFDM-ISAC system against multiple threats.

For simplicity of notation, we name the proposed design scheme as HBF Anti-PD&CA ISAC design scheme in the following numerical examples.

TABLE I
PARAMETER SETTINGS

Parameters	Value
Transmit/Receive Antennas	$M_t = M_r = 32$
RF Chains at Transmitter	$N_{RF} = 8$
No. of Downlink User	$U = 4$
Subcarriers	$K = 32$
System Center Frequency	$f_c = 10\text{GHz}$
System Bandwidth	$B = 2.56\text{GHz}$
Element Spacing of ULAs	$d = 0.0133\text{m}$
Transmit/Receive Power Budget	$P_{T,k} = P_{R,k} = 1, \forall k$
Noise Power of ER Aircraft	$\sigma_E^2 = -15\text{dB}$
Path Loss	$ \alpha_k ^2 = 5\text{dB}, \forall k$
Length of Analysis Window	$W = 16$
Noise Power of Communication	$\sigma_C^2 = -10\text{dB}$
Noise Power of Sensing	$\sigma_R^2 = -20\text{dB}$
Amplitude of ER Aircraft	$ \xi_E ^2 = 5\text{dB}$
Spatial Range	$[-90^\circ, 90^\circ]$
Spatial Sampling Number	$P = 181$

A. Simulation Setup

1) *Parameter Setting*: Unless otherwise specified, the parameter settings are provided in **Table I**. Assume that the advanced ER aircraft is possibly located within the angular interval $[28^\circ, 32^\circ]$, then its corresponding discrete angular set is $\Theta = [28^\circ, 29^\circ, 30^\circ, 31^\circ, 32^\circ]$. Besides, the CSI matrix from the OFDM-ISAC BS to the downlink communication user is constructed by the mmWave channel model in [40]–[42].

2) *Benchmark Specification*: For comparison purposes, several benchmarks are included in this paper.

- **HBF Radar Only**: This scheme considers a BS with HBF only works for target sensing.
- **HBF Anti-PD ISAC**: This scheme considers a secure BS with HBF for ISAC against only the PD intercept threat.
- **FD Anti-PD&CA ISAC**: This scheme considers a secure BS with FD for ISAC against both PD and CA intercept threats, as the upper bound of the proposed HBF Anti-PD&CA ISAC scheme.

B. Simulation Results

1) *Convergence of the Proposed Algorithm*: Fig. 3 shows the convergence curves of the proposed algorithm, with the radar SNR threshold is $\Gamma = 8\text{dB}$ and the communication QoS requirement is $\xi_{k,u} = \xi = 1\text{bps/Hz}, \forall k, u$. As can be seen in Fig. 3(a), as the iteration number¹ increases, the curve of the objective function gradually increases and then reaches a stationary value, while the curves of residual errors decrease to extremely low values. This validates the convergence of the proposed algorithm. Meanwhile, it can be observed from Fig. 3(b) and Fig. 3(c) that the curves of the achievable radar SNR and communication rates initially oscillate and approach the thresholds as the iteration number increases. This demonstrates the effectiveness of the proposed algorithm in guaranteeing communication and sensing performance.

2) *Performance of Combating PD*: Fig. 4 compares the maximum power collected by the ER aircraft across the uncertainty angular region versus the radar SNR threshold

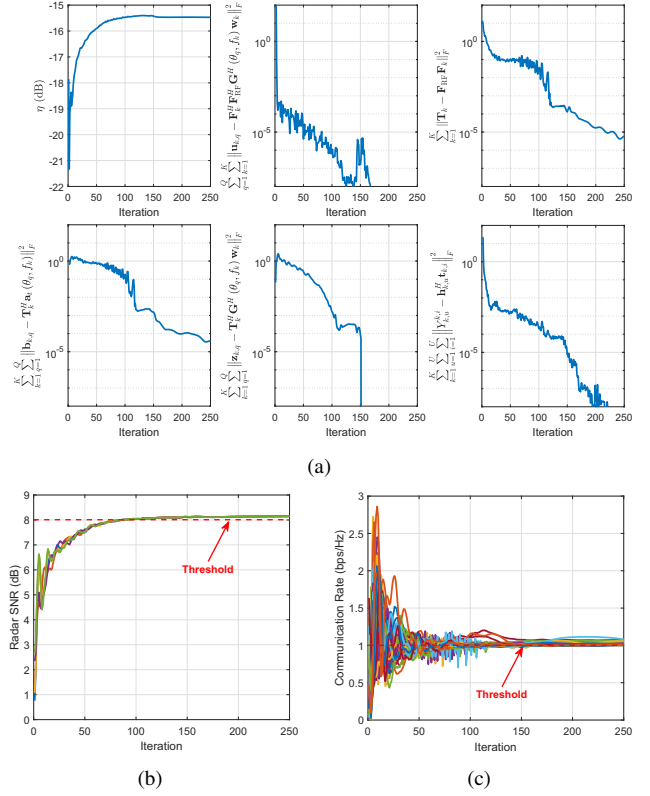


Fig. 3. Convergence performance of the proposed algorithm: (a) Objective function/residual errors versus the iteration number. (b) Radar SNR versus the iteration number. (c) Communication rate versus the iteration number.

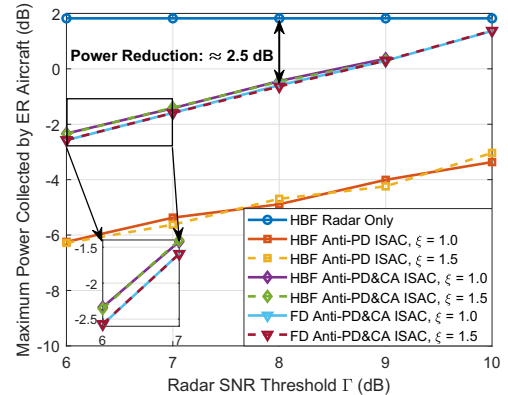


Fig. 4. Maximum power collected by the ER aircraft versus the radar SNR threshold obtained by different design schemes, with communication rate thresholds $\xi = 1.0, 1.5$.

with the communication rate threshold $\xi = 1.0, 1.5\text{bps/Hz}$. It can be observed that the power collected by the ER aircraft of all the ISAC schemes is increasing with the radar SNR threshold, where the proposed scheme has about 2.5dB power reduction for the HBF Radar Only scheme at $\Gamma = 8\text{dB}$. This demonstrates that the proposed scheme has a satisfactory performance in combating the PD intercept threats. Besides, the power corresponding to the HBF Anti-PD&CA ISAC scheme is close to that of the FD Anti-PD&CA ISAC scheme. This verifies the effectiveness of the proposed HBF design. We can also see that the curves of the same scheme with $\xi = 1.0$ and $\xi = 1.5$ are almost overlapped. This shows that the different communication requirements only have a slight impact on the power collected by the ER aircraft. However, the

¹The iteration number mentioned in the numerical examples refers to the iteration number for the outer loop.

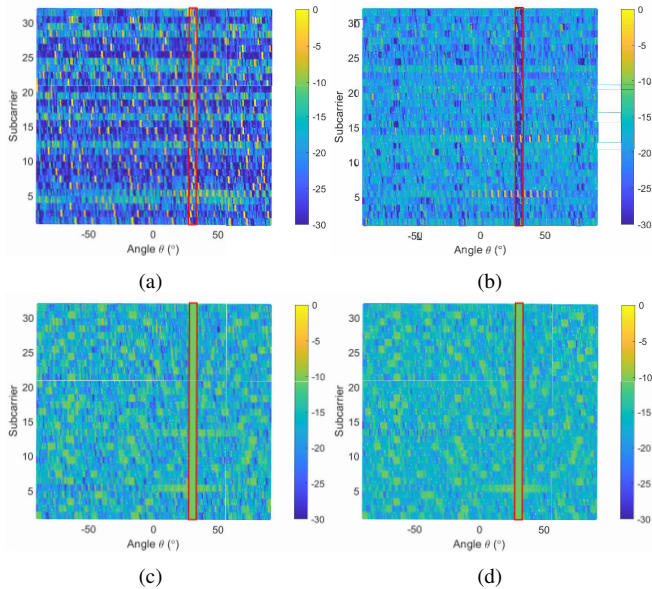


Fig. 5. Comparison of space-frequency spectra obtained by different design schemes. (a) HBF Radar Only scheme. (b) HBF Anti-PD ISAC scheme. (c) HBF Anti-PD&CA ISAC scheme. (d) FD Anti-PD&CA ISAC scheme.

curves of the HBF Anti-PD&CA ISAC scheme are higher than those of the HBF Anti-PD ISAC scheme. This indicates that the additional design consideration for combating CA would sacrifice the performance for combating PD to some extent.

3) *Space-Frequency Spectrum*: Fig. 5 compares the space-frequency spectra obtained by different design schemes. In Fig. 5(c) and Fig. 5(d), we can observe that the space-frequency spectra obtained by the proposed HBF Anti-PD&CA ISAC scheme and the FD Anti-PD&CA ISAC scheme maintain an identically lower than -10dB level within $[28^\circ, 32^\circ]$. The HBF Radar Only scheme generates many peak levels within $[28^\circ, 32^\circ]$ as shown in Fig. 5(a) while the HBF Anti-PD ISAC scheme generates several higher than -5dB levels within $[28^\circ, 32^\circ]$ as shown in Fig. 5(b). This demonstrates that the proposed design can realize satisfactory space-frequency spectrum performance, maintaining the same relatively low level within the whole uncertain angular region where the advanced ER aircraft probably exists.

4) *Cyclic Spectrum*: Fig. 6 compares the cyclic spectra extracted by the advanced ER aircraft for different design schemes with the uncertain discrete angular set Θ . It can be seen that the cyclic spectra obtained by the proposed HBF Anti-PD&CA ISAC scheme and the FD Anti-PD&CA ISAC scheme only have peaks when the normalized cyclic frequency is 0, while the cyclic spectra obtained by the HBF Radar Only scheme and the HBF Anti-PD ISAC scheme have some peaks in other regions. Besides, all the cyclic spectra obtained by the proposed scheme with Θ have high similarity with that of the AWGN in Fig. 2. This validates the effectiveness and superiority of the proposed design over the existing design in combating CA intercept threat via generating a noise-like cyclic spectrum.

5) *Impact of Target Location Uncertainty*: Then, we provide more numerical examples to further evaluate the system performance under different target location uncertainties. Fig. 7 plots the maximum power collected by the ER aircraft for

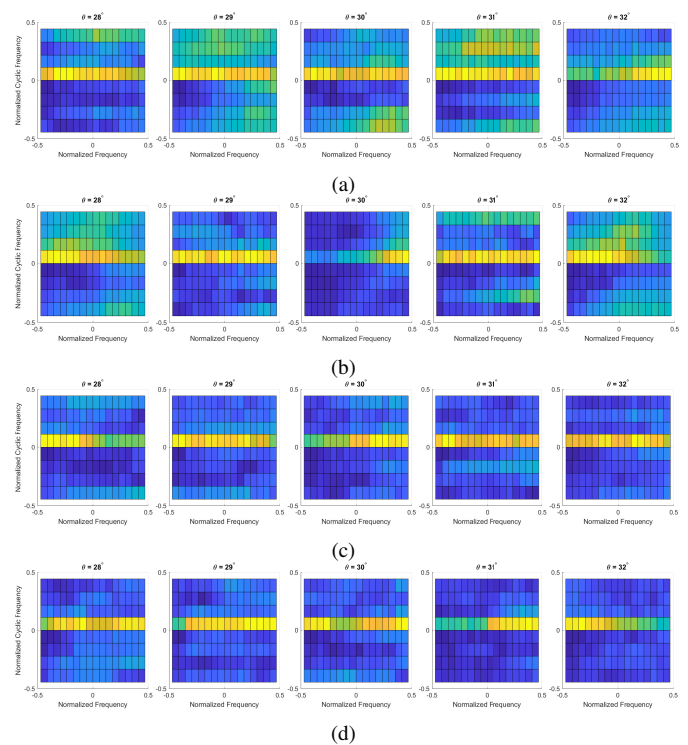


Fig. 6. Comparisons of cyclic spectra extracted by the advanced ER aircraft for different design schemes with the uncertain discrete angular set Θ . (a) HBF Radar Only scheme. (b) HBF Anti-PD ISAC scheme. (c) HBF Anti-PD&CA ISAC scheme. (d) FD Anti-PD&CA ISAC scheme.

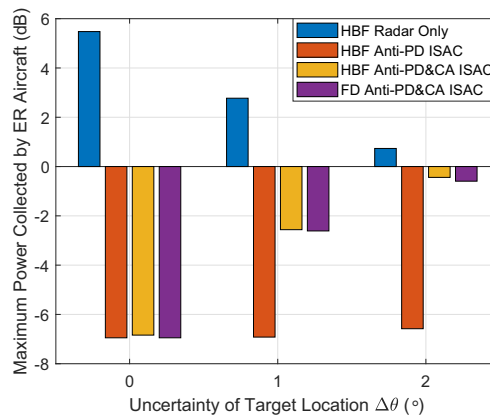


Fig. 7. Comparison of the maximum power collected by the ER aircraft under different uncertainties of target location $\Delta\theta = 0^\circ, 1^\circ, 2^\circ$.

different design schemes under different uncertainties of target location $\Delta\theta = 0^\circ, 1^\circ, 2^\circ$. As can be observed, when the uncertainty of target location is increasing, the maximum power collected by the ER aircraft for the HBF Radar Only scheme is decreasing while those for other schemes are increasing. Besides, the power difference between the HBF Anti-PD ISAC scheme and the proposed HBF Anti-PD&CA ISAC scheme becomes larger when the uncertainty of target location gets higher. This shows that the power reduction performance of the proposed Anti-PD&CA scheme degrades when the uncertainty of target location is increased.

Fig. 8 illustrates the space-frequency spectra obtained by the proposed design scheme under different uncertainties of target location $\Delta\theta = 0^\circ, 1^\circ, 2^\circ$. We can observe that the power radiated to the ER aircraft under $\Delta\theta = 0^\circ$ is almost the same

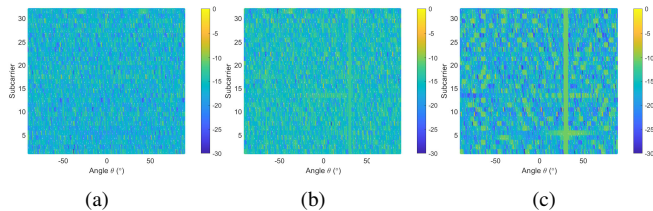


Fig. 8. Space-frequency spectra obtained by the proposed design scheme under different uncertainties of target location $\Delta\theta = 0^\circ, 1^\circ, 2^\circ$.

with other directions, those under $\Delta\theta = 1^\circ$ are similar to other directions, and those under $\Delta\theta = 2^\circ$ are slightly higher than others but still at a relatively low level. This shows that the proposed design can realize a slight level difference between the ER aircraft direction and other directions under different target location uncertainties.

Fig. 9 compares the cyclic spectra extracted by the ER aircraft at $\theta_0 = 30^\circ$ utilizing different design schemes with different uncertainties of target location $\Delta\theta = 0^\circ, 1^\circ, 2^\circ$. We can notice that when $\Delta\theta = 0^\circ$, the cyclic spectra for all the design schemes are similar to the cyclic spectra of the AWGN as shown in Fig. 2. As the uncertainty of the target location increases, the cyclic spectra resulting from the proposed HBF Anti-PD&CA ISAC scheme and the FD Anti-PD&CA ISAC scheme still resemble that of the AWGN while the HBF Radar Only scheme and the HBF Anti-PD ISAC scheme have several peaks at other normalized cyclic frequencies. This validates the feasibility of the proposed design in combating CA with target location uncertainty.

6) *Impact of the Number of RF Chains*: Furthermore, we evaluate the performance of the proposed HBF Anti-PD&CA ISAC design scheme by implementing the different number of RF chains. Specifically, the proposed algorithm is compiled under the different number of RF chains by applying the Monte Carlo method, and the constraint satisfaction probabilities of radar and communication performance are respectively calculated. Fig. 10 plots the constraint satisfaction probability of the proposed design scheme with the different number of RF chains N_t from the perspective of radar and communication performance. In Fig. 10(a), we can observe that the proposed design with fewer RF chains has the lower radar constraint satisfaction probability and even has “0%” radar constraint satisfaction probability when setting higher Γ . In Fig. 10(b), we can observe that the proposed design with $N_t = 4, 6$ RF chains fail to meet the communication QoS constraint, and the communication constraint satisfaction probabilities of higher RF chains become lower with higher ξ . Therefore, it indicates that it is necessary to choose a suitable number of RF chains to guarantee system performance in addition to reducing hardware costs.

VII. CONCLUSION

In this paper, we investigated improving the sensing security of OFDM-ISAC systems in the presence of an advanced ER aircraft that employs both PD and CA intercept methods. We first analyzed the power distribution and cyclic spectrum of ISAC signals, which are vital parameters involved in the decision-making mechanism for PD and CA, respectively.

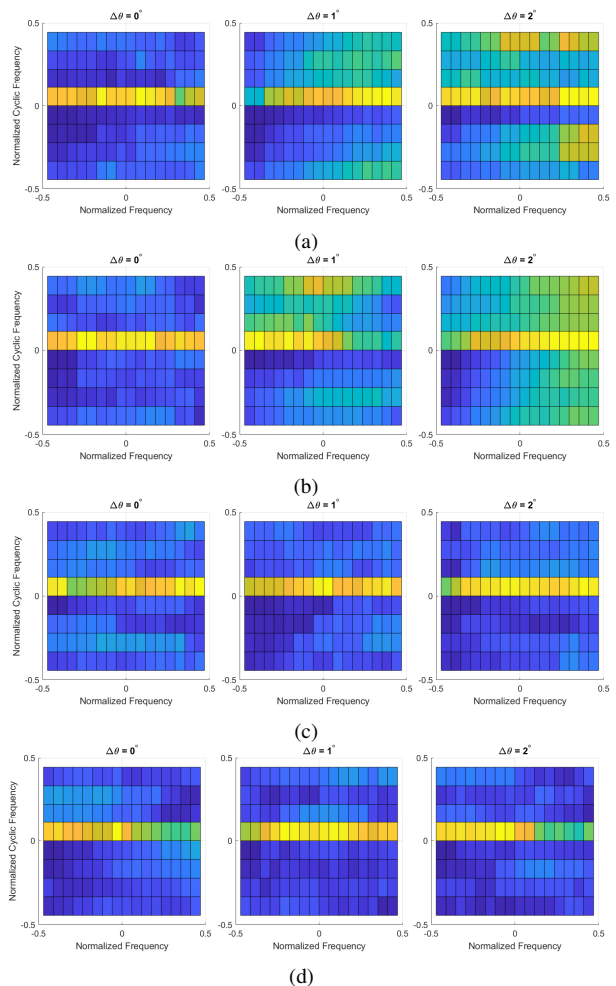


Fig. 9. Comparisons of cyclic spectra extracted by the ER aircraft utilizing different design schemes with different uncertainty of target location $\Delta\theta = 0^\circ, 1^\circ, 2^\circ$: (a) HBF Radar Only scheme. (b) HBF Anti-PD ISAC scheme. (c) HBF Anti-PD&CA ISAC scheme. (d) FD Anti-PD&CA ISAC scheme.

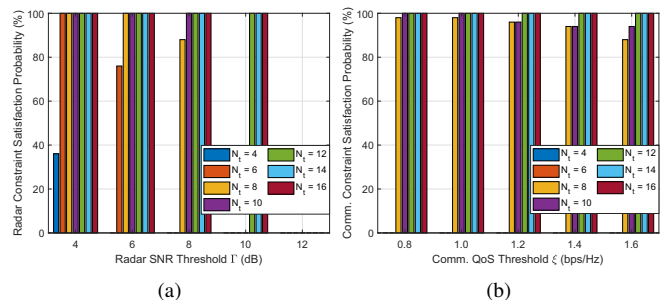


Fig. 10. Constraint satisfaction probability of the proposed design employing the different number of RF chains. (a) Radar performance. (b) Communication performance.

Specifically, we analyzed the intrinsic mathematical properties of a newly introduced metric, ergodic cyclic spectrum, to characterize the cyclostationary behavior. To enhance sensing security for ISAC signals, we devised an LPI-aware joint design of transmit HBF and radar receive filter by minimizing the probability of intercept subject to radar detection, communication QoS, power, and hardware constraints. To deal with the uncertainty of the target location and the unavailability of a specific ER decision-making mechanism, we devised a robust LPI design scheme and proposed an effective algorithm

based on the alternating optimization approach. Numerical simulations verify the convergence and effectiveness of the proposed algorithm. Moreover, it demonstrates that the proposed LPI-aware HBF design for the OFDM-ISAC system can enhance the system security against multi-intercept threats while guaranteeing satisfactory radar detection and communication performance.

APPENDIX A PROOF OF LEMMA 1

For the problem (26), once t is provided, $\mathbf{u}_{k,q}$ is set as the variable while others ($\mathbf{u}_{i,j}, i \neq k, j \neq q$) are held fixed. Specifically, $\mathbf{u}_{k,q}$ can be updated by solving

$$\min_{\mathbf{u}_{k,q}} \|\mathbf{u}_{k,q} - \tilde{\mathbf{v}}_{k,q}\|_F^2 \text{ s.t. } \sum_{k=1}^K \|\mathbf{u}_{k,q}\|_F^2 \geq t, \forall q. \quad (\text{A-1})$$

The objective function in (A-1) can be written as

$$\begin{aligned} \|\mathbf{u}_{k,q} - \tilde{\mathbf{v}}_{k,q}\|_F^2 &= \|\mathbf{u}_{k,q}\|_F^2 + \|\tilde{\mathbf{v}}_{k,q}\|_F^2 \\ &\quad - 2\|\mathbf{u}_{k,q}\|_F \|\tilde{\mathbf{v}}_{k,q}\|_F \Re \left\{ \left\langle \frac{\mathbf{u}_{k,q}}{\|\mathbf{u}_{k,q}\|_F}, \frac{\tilde{\mathbf{v}}_{k,q}}{\|\tilde{\mathbf{v}}_{k,q}\|_F} \right\rangle \right\}. \end{aligned} \quad (\text{A-2})$$

Since the maximum value of the inner product is achieved when

$$\frac{\mathbf{u}_{k,q}}{\|\mathbf{u}_{k,q}\|_F} = \frac{\tilde{\mathbf{v}}_{k,q}}{\|\tilde{\mathbf{v}}_{k,q}\|_F} \quad (\text{A-3})$$

we substitute (A-3) into (A-2) and have

$$\|\mathbf{u}_{k,q} - \tilde{\mathbf{v}}_{k,q}\|_F^2 = \|\mathbf{u}_{k,q}\|_F^2 - 2\|\mathbf{u}_{k,q}\|_F \|\tilde{\mathbf{v}}_{k,q}\|_F + \|\tilde{\mathbf{v}}_{k,q}\|_F^2. \quad (\text{A-4})$$

Now, taking constraint in (A-1) into consideration, the problem (26) can be converted into

$$\min_{\|\mathbf{u}_{k,q}\|_F} \left(\|\mathbf{u}_{k,q}\|_F - \|\tilde{\mathbf{v}}_{k,q}\|_F \right)^2 \text{ s.t. } \sum_{k=1}^K \|\mathbf{u}_{k,q}\|_F^2 \geq t, \forall q, \quad (\text{A-5})$$

whose solution can be easily derived as

$$\mathbf{u}_{k,q} = \begin{cases} \tilde{\mathbf{v}}_{k,q} & , \|\tilde{\mathbf{v}}_{k,q}\|_F \geq t \\ t^{1/2} \frac{\tilde{\mathbf{v}}_{k,q}}{\|\tilde{\mathbf{v}}_{k,q}\|_F} & , \text{otherwise} \end{cases}, \quad (\text{A-6})$$

with (A-3) being also held, where $\tilde{\mathbf{V}}_q = [\tilde{\mathbf{v}}_{1,q}, \dots, \tilde{\mathbf{v}}_{K,q}]$.

After $\mathbf{u}_{k,q}$ has been updated by (A-6), we substitute it into the problem (26), leading to

$$\min_t f(t) = -t + \frac{\mu}{2} \sum_{q=1}^Q \sum_{k=1}^K \beta_{q,k} \left(t^{1/2} - \|\tilde{\mathbf{V}}_q\|_F \right)^2, t > 0, \quad (\text{A-7})$$

where $\beta_q = 0$ if $\|\tilde{\mathbf{V}}_q\|_F \geq t$; otherwise, $\beta_q = 0$. The first-order and second-order derivatives of $f(t)$ can be given by

$$\frac{\partial f(t)}{\partial t} = -1 + \frac{\mu}{2} \sum_{q=1}^Q \sum_{k=1}^K \beta_{q,k} \left(1 - t^{-1/2} \|\tilde{\mathbf{V}}_q\|_F \right), \quad (\text{A-8a})$$

$$\frac{\partial^2 f(t)}{\partial t^2} = \frac{\mu}{4} \sum_{q=1}^Q \sum_{k=1}^K \beta_{q,k} t^{-3/2} \|\tilde{\mathbf{V}}_q\|_F \geq 0. \quad (\text{A-8b})$$

Based on (A-8b), $\frac{\partial f(t)}{\partial t}$ is monotonically increasing, w.r.t. $t > 0$. Thus, the optimal t can be easily obtained by solving $\frac{\partial f(t)}{\partial t} = 0$ with Newton's or bisection method.

The proof is completed.

APPENDIX B PROOF OF LEMMA 2

The Lagrange function of the problem (29) is given by

$$\begin{aligned} \mathcal{L}_{R,2,k}(\mathbf{w}_k, \kappa_k) &= \kappa_k \left(\|\mathbf{w}_k\|_F^2 - \mathcal{P}_{R,k} \right) \\ &\quad + \sum_{q=1}^Q \left\| \mathbf{u}_{k,q} - \mathbf{F}_k^H \mathbf{F}_{\text{RF}}^H \mathbf{A}^H(\theta_q, f_k) \mathbf{w}_k + \boldsymbol{\nu}_{k,q} \right\|_F^2, \end{aligned} \quad (\text{B-1})$$

where κ_k is a Lagrange multiplier associated with the constraint $\|\mathbf{w}_k\|_F^2 = \mathcal{P}_{R,k}$. The corresponding Karush-Kuhn-Tucker (KKT) conditions can be expressed as

$$\nabla_{\mathbf{w}_k} \mathcal{L}_{R,2,k}(\mathbf{w}_k, \kappa_k) = 0, \quad (\text{B-2a})$$

$$\|\mathbf{w}_k\|_F^2 - \mathcal{P}_{R,k} = 0. \quad (\text{B-2b})$$

Based on (B-2a), the optimal solution can be obtained by

$$\mathbf{w}_k(\kappa_k) = \left(\tilde{\mathbf{G}}_k + \kappa_k \mathbf{I}_{M_t} \right)^{-1} \tilde{\mathbf{\Phi}}_k, \quad (\text{B-3})$$

where $\tilde{\mathbf{G}}_k = \sum_{q=1}^Q \mathbf{A}(\theta_q, f_k) \mathbf{F}_{\text{RF}} \mathbf{F}_k \mathbf{F}_k^H \mathbf{F}_{\text{RF}}^H \mathbf{A}^H(\theta_q, f_k)$, $\tilde{\mathbf{\Phi}}_k = \sum_{q=1}^Q \mathbf{A}(\theta_q, f_k) \mathbf{F}_{\text{RF}} \mathbf{F}_k (\mathbf{u}_{k,q} + \boldsymbol{\nu}_{k,q})$.

To find the optimal κ_k , we make the eigen-decomposition of $\tilde{\mathbf{G}}_k$ as $\tilde{\mathbf{G}}_k = \tilde{\mathbf{G}}_k \tilde{\Sigma}_k \tilde{\mathbf{G}}_k^H$ and rewrite (B-3) as $\mathbf{w}_k(\kappa_k) = \tilde{\mathbf{G}}_k (\tilde{\Sigma}_k + \kappa_k \mathbf{I}_{M_t})^{-1} \tilde{\mathbf{G}}_k^H \tilde{\mathbf{\Phi}}_k$. Substituting into the receive power constraint, we obtain

$$\sum_{n=1}^{M_r} \frac{[\tilde{\mathbf{G}}_k^H \tilde{\mathbf{\Phi}}_k \tilde{\mathbf{\Phi}}_k^H \tilde{\mathbf{G}}_k]_{n,n}}{(\kappa_k + [\tilde{\Sigma}_k]_{n,n})^2} = P_{R,k}, \quad (\text{B-4})$$

where the left-hand term is monotonically decreasing, w.r.t., $\kappa_k > 0$, the optimal κ_k can be found by Newton's or bisection method. Accordingly, the optimal \mathbf{w}_k can be obtained.

The proof is completed.

REFERENCES

- [1] F. Liu, Y. Cui, C. Masouros *et al.*, "Integrated sensing and communications: Toward dual-functional wireless networks for 6G and beyond," *IEEE J. Sel. Areas Commun.*, vol. 40, no. 6, pp. 1728–1767, 2022.
- [2] Z. Wei, H. Qu, Y. Wang *et al.*, "Integrated sensing and communication signals toward 5G-A and 6G: A survey," *IEEE Internet Things J.*, vol. 10, no. 13, pp. 11 068–11 092, 2023.
- [3] Y. Cui, F. Liu, X. Jing, and J. Mu, "Integrating sensing and communications for ubiquitous IoT: Applications, trends, and challenges," *IEEE Netw.*, vol. 35, no. 5, pp. 158–167, 2021.
- [4] W. Saad, M. Bennis, and M. Chen, "A vision of 6G wireless systems: Applications, trends, technologies, and open research problems," *IEEE Netw.*, vol. 34, no. 3, pp. 134–142, 2019.
- [5] C.-X. Wang, X. You, X. Gao, X. Zhu, Z. Li, C. Zhang, H. Wang, Y. Huang, Y. Chen, H. Haas *et al.*, "On the road to 6G: Visions, requirements, key technologies, and testbeds," *IEEE Commun. Surveys Tuts.*, vol. 25, no. 2, pp. 905–974, 2023.
- [6] M. Giordani, M. Polese, M. Mezzavilla, S. Rangan, and M. Zorzi, "Toward 6G networks: Use cases and technologies," *IEEE Commun. Mag.*, vol. 58, no. 3, pp. 55–61, 2020.
- [7] Y. Zou, J. Zhu, X. Wang, and L. Hanzo, "A survey on wireless security: Technical challenges, recent advances, and future trends," *Proc. IEEE*, vol. 104, no. 9, pp. 1727–1765, 2016.
- [8] Y.-S. Shiu, S. Y. Chang, H.-C. Wu, S. C.-H. Huang, and H.-H. Chen, "Physical layer security in wireless networks: A tutorial," *IEEE Wireless Commun.*, vol. 18, no. 2, pp. 66–74, 2011.
- [9] A. Mukherjee, S. A. A. Fakoorian, J. Huang, and A. L. Swindlehurst, "Principles of physical layer security in multiuser wireless networks: A survey," *IEEE Commun. Surveys Tuts.*, vol. 16, no. 3, pp. 1550–1573, 2014.

- [10] Y. Liu, H.-H. Chen, and L. Wang, "Physical layer security for next generation wireless networks: Theories, technologies, and challenges," *IEEE Commun. Surveys Tuts.*, vol. 19, no. 1, pp. 347–376, 2016.
- [11] Z. Wei, F. Liu, C. Masouros, N. Su, and A. P. Petropulu, "Toward multi-functional 6G wireless networks: Integrating sensing, communication, and security," *IEEE Commun. Mag.*, vol. 60, no. 4, pp. 65–71, 2022.
- [12] Y. Jiang, L. Wang, H.-H. Chen, and X. Shen, "Physical layer covert communication in B5G wireless networks—its research, applications, and challenges," *Proc. IEEE*, 2024.
- [13] J. Chu, Z. Lu, R. Liu, M. Li, and Q. Liu, "Joint beamforming and reflection design for secure RIS-ISAC systems," *IEEE Trans. Veh. Technol.*, vol. 73, no. 3, pp. 4471–4475, 2023.
- [14] D. Xu, X. Yu, D. W. K. Ng, A. Schmeink, and R. Schober, "Robust and secure resource allocation for ISAC systems: A novel optimization framework for variable-length snapshots," *IEEE Trans. Commun.*, vol. 70, no. 12, pp. 8196–8214, 2022.
- [15] Z. Ren, L. Qiu, J. Xu, and D. W. K. Ng, "Robust transmit beamforming for secure integrated sensing and communication," *IEEE Trans. Commun.*, vol. 71, no. 9, pp. 5549–5564, 2023.
- [16] N. Su, F. Liu, and C. Masouros, "Secure radar-communication systems with malicious targets: Integrating radar, communications and jamming functionalities," *IEEE Trans. Wireless Commun.*, vol. 20, no. 1, pp. 83–95, 2020.
- [17] L. Guo, J. Jia, J. Chen, S. Yang, and X. Wang, "Secure Beamforming and Radar Association in CoMP-NOMA Empowered Integrated Sensing and Communication Systems," *IEEE Trans. Inf. Forensics Security*, 2024.
- [18] P. Liu, Z. Fei, X. Wang, B. Li, Y. Huang, and Z. Zhang, "Outage constrained robust secure beamforming in integrated sensing and communication systems," *IEEE Wireless Commun. Lett.*, vol. 11, no. 11, pp. 2260–2264, 2022.
- [19] L. Hu, H. Wen, B. Wu, F. Pan, R.-F. Liao, H. Song, J. Tang, and X. Wang, "Cooperative jamming for physical layer security enhancement in Internet of Things," *IEEE Internet Things J.*, vol. 5, no. 1, pp. 219–228, 2017.
- [20] J. Gu, G. Ding, H. Wang, and Y. Xu, "Robust beamforming for sensing assisted integrated communication and jamming systems," *IEEE Trans. Veh. Technol.*, vol. 72, no. 10, pp. 13 649–13 654, 2023.
- [21] R. Ye, Y. Peng, F. Al-Hazemi, and R. Boutaba, "A robust cooperative jamming scheme for secure UAV communication via intelligent reflecting surface," *IEEE Trans. Commun.*, vol. 72, no. 2, pp. 1005–1019, 2023.
- [22] P. Montezuma and R. Dinis, "Implementing physical layer security using transmitters with constellation shaping," in *2015 24th International Conference on Computer Communication and Networks (ICCCN)*. IEEE, 2015, pp. 1–4.
- [23] I. Bang and T. Kim, "Secure modulation based on constellation mapping obfuscation in OFDM based TDD systems," *IEEE Access*, vol. 8, pp. 197 644–197 653, 2020.
- [24] S. Ma, Y. Zhang, H. Sheng, H. Li, J. Shi, L. Yang, Y. Wu, N. Al-Dhahir, and S. Li, "Optimal probabilistic constellation shaping for covert communications," *IEEE Trans. Inf. Forensics Security*, vol. 17, pp. 3165–3178, 2022.
- [25] A. Stove, A. Hume, and C. Baker, "Low probability of intercept radar strategies," *IEE Proceedings-Radar, Sonar and Navigation*, vol. 151, no. 5, pp. 249–260, 2004.
- [26] P. E. Pace, *Detecting and classifying low probability of intercept radar*. Artech house, 2009.
- [27] Y. Liu, P. Xiao, H. Wu *et al.*, "LPI radar signal detection based on radial integration of Choi-Williams time-frequency image," *Journal of systems engineering and electronics*, vol. 26, no. 5, pp. 973–981, 2015.
- [28] M. Zhang, L. Liu, and M. Diao, "LPI radar waveform recognition based on time-frequency distribution," *Sensors*, vol. 16, no. 10, p. 1682, 2016.
- [29] C. Shi, F. Wang, S. Salous, and J. Zhou, "Low probability of intercept-based optimal OFDM waveform design strategy for an integrated radar and communications system," *IEEE Access*, vol. 6, pp. 57 689–57 699, 2018.
- [30] C. Shi, F. Wang, M. Sellathurai, J. Zhou, and S. Salous, "Low probability of intercept-based optimal power allocation scheme for an integrated multistatic radar and communication system," *IEEE Syst. J.*, vol. 14, no. 1, pp. 983–994, 2019.
- [31] Y. Wang, C. Shi, F. Wang, and J. Zhou, "LPI-based optimal radar power allocation for target time delay estimation in joint radar and communications system," in *2020 IEEE 11th Sensor Array and Multichannel Signal Process. Workshop (SAM)*, 2020, pp. 1–4.
- [32] P. Gong, Z. Zhang, Y. Wu, and W.-Q. Wang, "Joint design of transmit waveform and receive beamforming for LPI FDA-MIMO radar," *IEEE Signal Process. Lett.*, vol. 29, pp. 1938–1942, 2022.
- [33] A. Gupta and A. A. Bazil Rai, "Feature Extraction of Intra-Pulse Modulated LPI Waveforms Using STFT," in *2019 4th Int. Conf. on Recent Trends on Electron., Info., Commun. & Tech. (RTEICT)*, 2019, pp. 742–746.
- [34] E. R. Zilberman and P. E. Pace, "Autonomous time-frequency morphological feature extraction algorithm for LPI radar modulation classification," in *2006 Int. Conf. on Image Process.*, 2006, pp. 2321–2324.
- [35] R. K. Chilukuri, H. K. Kakarla, and K. Subbarao, "Estimation of modulation parameters of LPI radar using cyclostationary method," *Sensing and Imaging*, vol. 21, no. 1, p. 51, 2020.
- [36] X. Liu, Y. Yuan, T. Zhang *et al.*, "Integrated transmit waveform and RIS phase shift design for LPI detection and communication," *IEEE Trans. Wireless Commun.*, vol. 23, no. 6, pp. 5663–5679, 2023.
- [37] Q. Shi, Y. Wang, Z. Zhou, G. Cui, and P. Fan, "Low Probability of Intercept Signal Design for MIMO Integrated Sensing and Communication Systems," *IEEE Trans. Commun.*, 2025.
- [38] A. Alkhateeb, O. El Ayach, G. Leus, and R. W. Heath, "Channel estimation and hybrid precoding for millimeter wave cellular systems," *IEEE J. Sel. Topics Signal Process.*, vol. 8, no. 5, pp. 831–846, 2014.
- [39] A. F. Molisch, V. V. Ratnam, S. Han, Z. Li, S. L. H. Nguyen, L. Li, and K. Haneda, "Hybrid beamforming for massive MIMO: A survey," *IEEE Commun. Mag.*, vol. 55, no. 9, pp. 134–141, 2017.
- [40] W. Deng, M. Li, M.-M. Zhao *et al.*, "CSI Transfer From Sub-6G to mmWave: Reduced-Overhead Multi-User Hybrid Beamforming," *IEEE J. Sel. Areas Commun.*, vol. 43, no. 3, pp. 973–987, 2025.
- [41] Z. Cheng, Z. He, and B. Liao, "Hybrid beamforming design for OFDM dual-function radar-communication system," *IEEE J. Sel. Topics Signal Process.*, vol. 15, no. 6, pp. 1455–1467, 2021.
- [42] H. Li, M. Li, Q. Liu *et al.*, "Dynamic hybrid beamforming with low-resolution PSs for wideband mmWave MIMO-OFDM systems," *IEEE J. Sel. Areas Commun.*, vol. 38, no. 9, pp. 2168–2181, 2020.
- [43] W. A. Gardner, "The spectral correlation theory of cyclostationary time-series," *Signal processing*, vol. 11, no. 1, pp. 13–36, 1986.
- [44] X. Liu, T. Zhang, X. Yu *et al.*, "LPI waveform design for radar system against cyclostationary analysis intercept processing," *Signal Processing*, vol. 201, p. 108681, 2022.
- [45] X. Liu, T. Zhang, Q. Shi *et al.*, "LPI radar waveform design with desired cyclic spectrum and pulse compression properties," *IEEE Trans. Veh. Technol.*, vol. 72, no. 5, pp. 6789–6793, 2023.
- [46] A. De Maio, S. De Nicola, Y. Huang *et al.*, "Design of phase codes for radar performance optimization with a similarity constraint," *IEEE Trans. Signal Process.*, vol. 57, no. 2, pp. 610–621, 2008.
- [47] L. Xu, B. Wang, and Z. Cheng, "Task-Oriented Hybrid Beamforming for OFDM-DFRC Systems With Flexibly Controlled Space-Frequency Spectra," *IEEE Trans. on Cogn. Commun. Netw.*, 2024.